Inorganic Chemistry

Article

pubs.acs.org/IC

Osmium Bisterpyridine Complexes with Redox-Active Amine Substituents: A Comparison Study with Ruthenium Analogues

Meng-Jia Sun, Jiang-Yang Shao,* Chang-Jiang Yao, Yu-Wu Zhong,* and Jiannian Yao*

Beijing National Laboratory for Molecular Sciences, CAS Key Laboratory of Photochemistry, Institute of Chemistry, Chinese Academy of Sciences, Beijing 100190, China

Supporting Information

ABSTRACT: Five osmium complexes with redox-active amine substituents, [Os(ttpy)(Ntpy)]$(PF_6)_2$ ($\mathbf{1}(PF_6)_2$), [Os(Ntpy)$_2$]$(PF_6)_2$ ($\mathbf{2}(PF_6)_2$), [Os(ttpy)(NPhtpy)]$(PF_6)_2$ ($\mathbf{3}(PF_6)_2$), [Os(Ntpy)(NPhtpy)]$(PF_6)_2$ ($\mathbf{4}(PF_6)_2$), and [Os(NPhtpy)$_2$]$(PF_6)_2$ ($\mathbf{5}(PF_6)_2$), have been prepared, where ttpy is 4′-tolyl-2,2′:6′,2″-terpyridine, Ntpy is 4′-(di-*p*-anisylamino)-2,2′:6′,2″-terpyridine, and NPhtpy is 4′-(di-*p*-anisylaminophen-4-yl)-2,2′:6′,2″-terpyridine. X-ray crystallographic data of $\mathbf{2}(PF_6)_2$ and $\mathbf{4}(PF_6)_2$ are presented. These complexes show rich visible absorptions attributed to the singlet metal-to-ligand charge-transfer (^{1}MLCT), triplet MLCT, and intraligand charge-transfer transitions. Complexes $\mathbf{3}(PF_6)_2$ and $\mathbf{5}(PF_6)_2$ show weak emissions around 720 nm at room temperature. All complexes show stepwise oxidations of the osmium ion and the amine segment. However, the redox potentials and the order of the $Os^{III/II}$ and $N^{\bullet+/0}$ processes vary significantly, depending on the electronic nature of the amine substituents. In the singly oxidized state, either Os(II) → $N^{\bullet+}$ MLCT or N → Os(III) ligand-to-metal charge-transfer transitions in the near-infrared region have been observed. For complexes $\mathbf{2}(PF_6)_2$, $\mathbf{4}(PF_6)_2$, and $\mathbf{5}(PF_6)_2$ with two amine substituents, no evidence has been observed for the presence of osmium-mediated amine−amine electronic coupling. Density functional theory (DFT) and time-dependent DFT calculations have been performed to complement these experimental results. The one-electron-oxidized forms $\mathbf{3}^{3+}$ and $\mathbf{5}^{3+}$ show distinct electron paramagnetic resonance (EPR) signals in CH_3CN at room temperature. However, complexes $\mathbf{1}^{3+}$, $\mathbf{2}^{3+}$, and $\mathbf{4}^{3+}$ are EPR silent under similar conditions. In addition, a comparison study has been made between these osmium complexes and the previously reported ruthenium analogues.

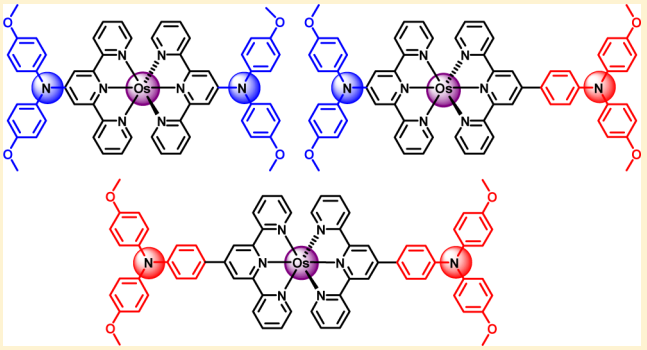

INTRODUCTION

Molecular materials with multiple redox-active components are useful for a wide range of applications, such as molecular electronics,[1] electrochromism,[2] information storage,[3] ion sensing,[4] molecular magnetism,[5] charge-transporting,[6] light absorption and solar cells,[7] and mixed-valent chemistry.[8] Transition-metal complexes decorated with additional redox-active motifs are one type of such materials that display intriguing electrochemical and photophysical properties and are potentially useful for the above-mentioned applications. In this context, many complexes containing various redox-active motifs, such as tetrathiafulvalene,[9] triarylamine,[10] carbazole,[11] triarylborane,[12] ferrocene,[13] or an organic radical,[14] have been reported. It should be noted that most of these known examples focus on ruthenium complexes, partially because of their ease of preparation and good stability. In comparison, osmium complexes containing additional redox-active sites have received much less attention.

Compared with ruthenium complexes, the third-row osmium complexes generally have more-inert metal−ligand bonds. The reaction conditions for the synthesis of osmium complexes are often much harsher with respect to those for ruthenium complexes. In addition, one distinguished feature of the third-row elements is their enhanced spin−orbit coupling relative to the second-row elements, which makes the optoelectronic properties of osmium complexes significantly different from those of ruthenium complexes. To date, a number of osmium complexes have been synthesized and studied regarding their photophysical properties and electron-transfer behavior.[15] It would be interesting to examine the modulation of these properties by the additional redox-active motifs present in the same molecule.

We present herein a combined experimental and theoretical study of five osmium−bisterpyridine complexes, $\mathbf{1}(PF_6)_2$−$\mathbf{5}(PF_6)_2$, containing one or two redox-active amine substituents (Figure 1). Either the amine substituents are directly connected to the central pyridine ring of terpyridine, or a phenyl group is inserted between the amine nitrogen atom and the pyridine ring. We previously found that the amine oxidation potentials (the $N^{\bullet+/0}$ process) in these two situations differ significantly.[16] The electrochemical and photophysical properties of these

Received: June 24, 2015
Published: August 3, 2015

DOI: 10.1021/acs.inorgchem.5b01420
Inorg. Chem. 2015, 54, 8136−8147

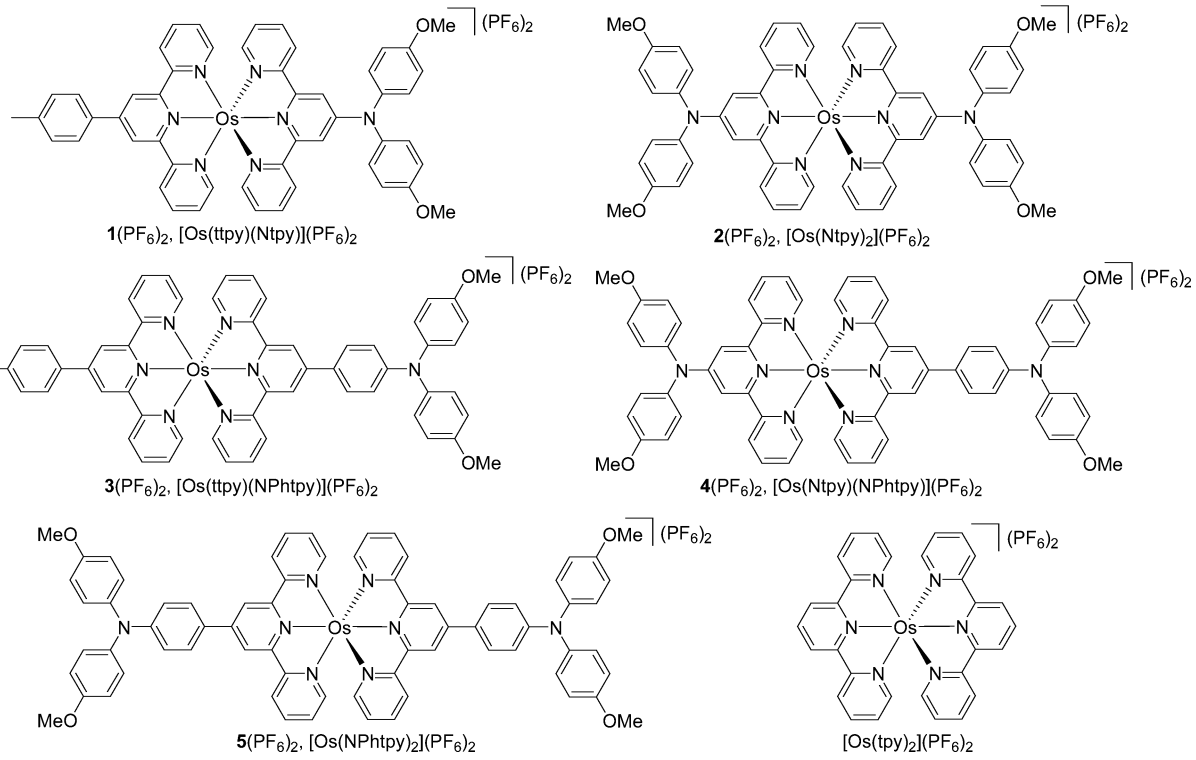

Figure 1. Compounds studied in this paper.

complexes are examined and compared with those of the previously reported ruthenium analogues.[16,17] In addition, oxidative spectroelectrochemical measurements have been performed to probe the charge-transfer properties of the resulting singly or doubly oxidized forms. Finally, density functional theory (DFT) and time-dependent DFT (TDDFT) calculations have been performed to complement these experimental results.

RESULTS AND DISCUSSION

Synthesis and Single-Crystal Structures. In order to prepare complexes $\mathbf{1}(PF_6)_2$–$\mathbf{5}(PF_6)_2$, three known tridentate ligands, 4′-tolyl-2,2′:6′,2″-terpyridine (ttpy),[18] 4′-(di-*p*-anisylamino)-2,2′:6′,2″-terpyridine (Ntpy),[17] and 4′-(di-*p*-anisylaminophen-4-yl)-2,2′:6′,2″-terpyridine (NPhtpy),[16] were first synthesized according to known procedures. The reaction of ttpy and NPhtpy with $[(NH_4)_2OsCl_6]$ in ethylene glycol at 160 °C for 1 h gave the $[(ttpy)OsCl_3]$ and the $[(NPhtpy)OsCl_3]$ salts,[15g] respectively, which were used for the next transformation without further purification. Complexes $\mathbf{1}(PF_6)_2$ and $\mathbf{3}(PF_6)_2$ were prepared from the reaction of $[(ttpy)OsCl_3]$ with Ntpy or NPhtpy, respectively, in refluxing ethylene glycol for 2 h, followed by anion exchange using KPF_6. The harsh conditions are necessary for the synthesis of osmium complexes. The triarylamine components are tolerated under these conditions. Similar conditions have been used for the synthesis of known osmium polypyridyl complexes.[15,19] In a similar way, the treatment of $[(NPhtpy)OsCl_3]$ with Ntpy gave the asymmetric diamine complex $\mathbf{4}(PF_6)_2$. The symmetric diamine complexes $\mathbf{2}(PF_6)_2$ and $\mathbf{5}(PF_6)_2$ were prepared from the reaction of $[(NH_4)_2OsCl_6]$ with 2 equiv of Ntpy or NPhtpy, respectively. The yields for the synthesis of these osmium complexes are moderate to good, varying from 68% to 91%. The synthesis details and characterization data of these compounds are given in the Experimental Section.

Single crystals of $\mathbf{2}(PF_6)_2$ and $\mathbf{4}(PF_6)_2$ were obtained by slowly diffusing diethyl ether into their solutions in CH_3CN. Their X-ray crystallographic structures are shown in Figure 2. The osmium ion has an expected hexa-coordinate octahedral configuration. The triarylamine motifs have a three-wheel propeller configuration. The distance between two amine nitrogen atoms of $\mathbf{2}(PF_6)_2$ is 12.31 Å, while that of $\mathbf{4}(PF_6)_2$ is 16.57 Å. The crystallographic data are shown in the Experimental Section and Supporting Information (SI).

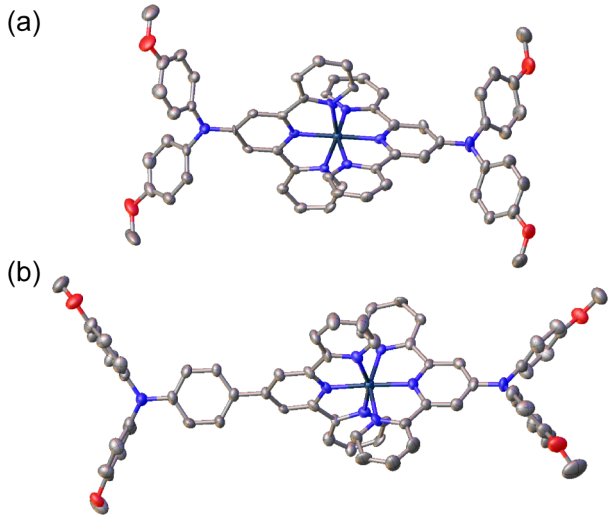

Figure 2. Thermal ellipsoid diagram (30% probability) of the single-crystal structure of (a) $\mathbf{2}(PF_6)_2$ and (b) $\mathbf{4}(PF_6)_2$. Hydrogen atoms and anions are omitted for clarity. Atom color code: carbon, gray; nitrogen, blue; oxygen, red; osmium, navy.

DOI: 10.1021/acs.inorgchem.5b01420
Inorg. Chem. 2015, 54, 8136–8147

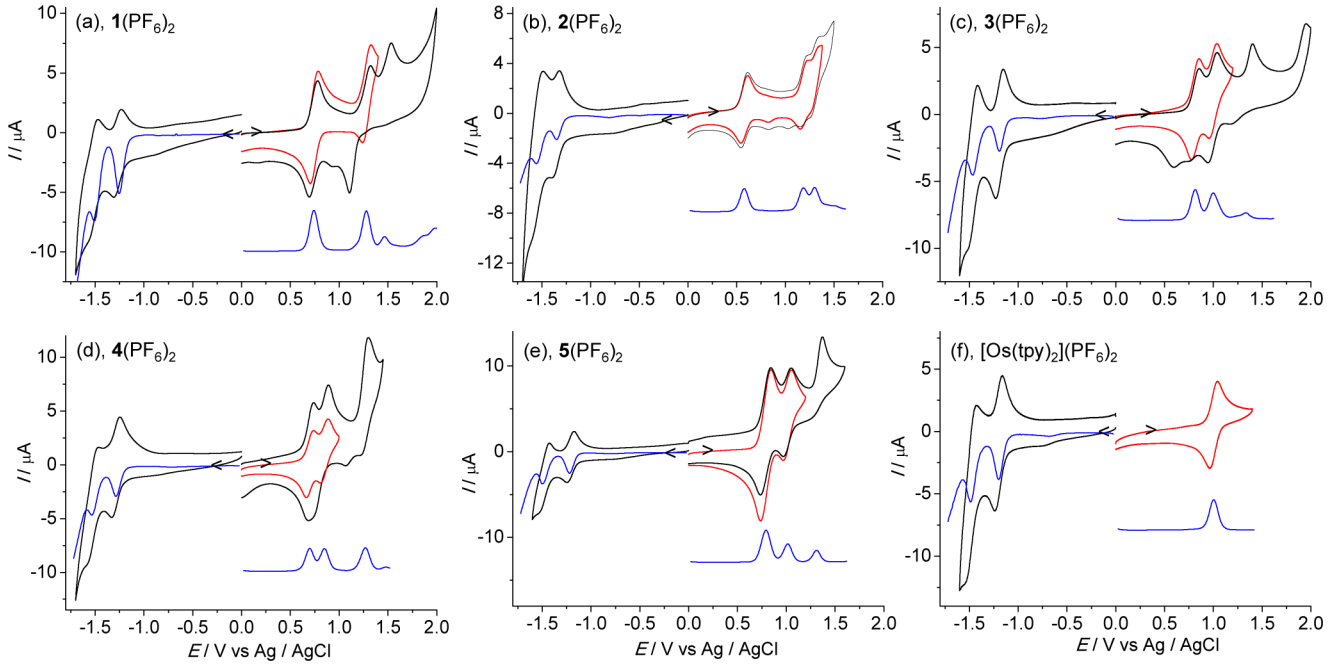

Figure 3. CVs (black and red curves) and DPVs (blue curves) of $\mathbf{1}(PF_6)_2$–$\mathbf{5}(PF_6)_2$ and $[Os(tpy)_2](PF_6)_2$ at a disk Pt electrode in 0.1 M Bu_4NClO_4/CH_3CN. For the sake of clarity, the anodic DPV curves are placed below the corresponding CVs.

Table 1. Electrochemical and Absorption Data[a]

compound	$E_{1/2}$/V anodic	$E_{1/2}$/V cathodic	$\lambda_{abs,max}$ [nm] ($\varepsilon \times 10^5$ M^{-1} cm^{-1})
Ntpy	+0.97, +1.41[b]		282 (0.46)
NPhtpy	+0.81, +1.25[b]		288 (0.38), 365 (0.27)
$\mathbf{1}(PF_6)_2$, $[Os(ttpy)(Ntpy)](PF_6)_2$	+0.74, +1.28, +1.53[b]	−1.27, −1.51	284 (0.83), 306 (0.79), 350 (0.24), 502 (0.28), 678 (0.066)
$[Ru(tpy)(Ntpy)](PF_6)_2$	+0.98, +1.35,[b] +1.44	−1.28, −1.52	274 (0.65), 303 (0.74), 495 (0.25)
$\mathbf{2}(PF_6)_2$, $[Os(Ntpy)_2](PF_6)_2$	+0.58, +1.19, +1.30	−1.35, −1.56	306 (0.77), 518 (0.23), 692 (0.75)
$[Ru(Ntpy)_2](PF_6)_2$	+0.96, +1.23, +1.56,[b] +1.64	−1.34, −1.58	302 (0.94), 350 (0.21), 512 (0.25)
$\mathbf{3}(PF_6)_2$, $[Os(ttpy)(NPhtpy)](PF_6)_2$	+0.82, +1.00, +1.40[b]	−1.20, −1.46	284 (0.51), 314 (0.69), 396 (0.15), 502 (0.31), 672 (0.078)
$[Ru(tpy)(NPhtpy)](PF_6)_2$	+0.82, +1.30,[b] +1.36	−1.24, −1.49	272 (0.33), 308 (0.50), 496 (0.20)
$\mathbf{4}(PF_6)_2$, $[Os(Ntpy)(NPhtpy)](PF_6)_2$	+0.70, +0.85, +1.30[b]	−1.28, −1.53	278 (0.67), 310 (0.81), 354 (0.35), 516 (0.36), 584 (0.085)
$[Ru(Ntpy)(NPhtpy)](PF_6)_2$	+0.82, +1.02, +1.31,[b] +1.36,[b] +1.48	−1.30, −1.54	277 (0.64), 301 (0.70), 515 (0.35)
$\mathbf{5}(PF_6)_2$, $[Os(NPhtpy)_2](PF_6)_2$	+0.79 (2e), +1.02, +1.31[b]	−1.22, −1.50	278 (0.58), 314 (0.85), 352 (0.43), 515 (0.45), 676 (0.12)
$[Ru(NPhtpy)_2](PF_6)_2$	+0.81 (2e), +1.30,[b] +1.37	−1.26, −1.46	275 (0.53), 310 (0.71), 404 (0.18), 516 (0.42)
$[Os(tpy)_2](PF_6)_2$	+1.01	−1.20, −1.48	270 (0.43), 310 (0.69), 476 (0.14), 662 (0.040)
$[Ru(tpy)_2](PF_6)_2$	+1.32	−1.22, −1.46	270 (0.48), 307 (0.78), 475 (0.17)

[a]Data in CH_3CN. The electrochemical potentials are reported as the $E_{1/2}$ value vs Ag/AgCl. Potentials vs ferrocene$^{+/0}$ can be estimated by subtracting 0.45 V. [b]Anodic peak potential of irreversible processes.

Electrochemical Studies. Figure 3 shows the cyclic voltammograms (CVs) and differential pulse votammograms (DPVs) of the above synthesized osmium complexes. The electrochemical data are summarized in Table 1, together with those of the ruthenium analogues for comparison. Ligands Ntpy and NPhtpy display a chemically reversible $N^{\bullet+/0}$ redox couple at +0.97 ($N_{Ntpy}^{\bullet+/0}$) and +0.81 V ($N_{NPhtpy}^{\bullet+/0}$) vs Ag/AgCl, respectively (Figure S1, SI). At more positive potentials, irreversible oxidation peaks are observed for both compounds. They are attributed to the further oxidation of the in situ generated aminium radical cation, namely the irreversible $N^{2+/\bullet+}$ process.[17,20] This feature is observed for all of these amine-containing complexes. When these two ligands are chelated with Ru(tpy) (tpy = 2,2′:6′,2″-terpyridine), the $N^{\bullet+/0}$ potentials only vary a little (+0.98 and +0.82 V for $[Ru(tpy)(Ntpy)](PF_6)_2$ and $[Ru(tpy)(NPhtpy)](PF_6)_2$, respectively) and the $Ru^{III/II}$ processes (+1.44 and +1.36 V, respectively) slightly shift to the more positive region relative to that of $[Ru(tpy)_2](PF_6)_2$ ($Ru_{[Ru(tpy)_2]}^{III/II}$, +1.32 V).[16]

The situations significantly changed in the osmium complexes. Complex $\mathbf{1}(PF_6)_2$ ($[Os(ttpy)(Ntpy)](PF_6)_2$) shows two anodic waves at +0.74 and +1.28 V. The first wave has a more than 200 mV shift to the less positive region with respect to either the $N_{Ntpy}^{\bullet+/0}$ process (+0.98 V) or the $Os^{III/II}$ process of $[Os(tpy)_2](PF_6)_2$ ($Os_{[Os(tpy)_2]}^{III/II}$, +1.01 V).[21] This may suggest that a stronger degree of electronic coupling is present between Ntpy and Os(tpy) relative to that between Ntpy and Ru(tpy). This is reminiscent of redox asymmetric mixed-valent systems where the electronic coupling is larger for compounds with smaller redox asymmetry between two distal redox sites.[22] The difference between the $N_{Ntpy}^{\bullet+/0}$ and the

DOI: 10.1021/acs.inorgchem.5b01420
Inorg. Chem. 2015, 54, 8136−8147

$Os_{[Os(tpy)_2]}^{III/II}$ potential is much smaller with respect to that between the $N_{Ntpy}^{\bullet+/0}$ and the $Ru_{[Ru(tpy)_2]}^{III/II}$ potential, which favors the electronic coupling between Ntpy and Os(tpy) components and thus leads to the obvious shift of the first redox couple of $\mathbf{1}(PF_6)_2$. For complex $\mathbf{2}(PF_6)_2$ with two Ntpy ligands, the first anodic wave shifts to an even less positive region (+0.58 V), followed by two closely spaced couples at +1.19 and +1.30 V. Later spectroelectrochemical experiments suggest that the first redox couple of $\mathbf{1}(PF_6)_2$ and $\mathbf{2}(PF_6)_2$ are more biased toward the oxidation of the osmium component. In this sense, the two well-separated waves at +1.19 and +1.30 V of $\mathbf{2}(PF_6)_2$ are possibly due to the stepwise oxidations of two amine substituents, which may be interpreted as the presence of electronic coupling between two amine sites through the Os^{III} bridge. However, the following theoretical studies suggest a different interpretation. In addition, the potentials of the first anodic waves of the Ntpy-containing complexes $\mathbf{1}(PF_6)_2$ and $\mathbf{2}(PF_6)_2$ are both less positive relative to those of the NPhtpy-containing complexes $\mathbf{3}(PF_6)_2$ and $\mathbf{5}(PF_6)_2$ (discussed below). This is very interesting considering that the $N_{Ntpy}^{\bullet+/0}$ potential is more positive relative to the $N_{NPhtpy}^{\bullet+/0}$ potential.

The first anodic redox wave of the NPhtpy-containing complexes $\mathbf{3}(PF_6)_2$ and $\mathbf{5}(PF_6)_2$ occurs at +0.82 and +0.79 V (2e process judging from the current height), respectively. By comparing the $N_{NPhtpy}^{\bullet+/0}$ potential (+0.81 V) and the $Os_{[Os(tpy)_2]}^{III/II}$ potential (+1.01 V), it is reasonable to assign these waves to the $N^{\bullet+/0}$ processes of the amine components. The subsequent redox waves at +1.00 V of $\mathbf{3}(PF_6)_2$ and +1.02 V of $\mathbf{5}(PF_6)_2$ thus belong to the $Os^{III/II}$ processes. This assignment is supported by following spectroscopic results and theoretical calculations. In this case, the change of the $N^{\bullet+/0}$ potential of the NPhtpy ligand is insignificant after chelation with osmium ion. This situation is very similar when the NPhtpy ligand is chelated with the ruthenium ion.[16] The appearance of the $N^{\bullet+/0}$ processes of $\mathbf{5}(PF_6)_2$ as a 2e wave at +0.79 V suggests that little electronic coupling is present between two amine units. No intervalence charge-transfer (IVCT) transition has been observed in the following spectroelectrochemical measurements either. This situation is also similar to the ruthenium analogue $[Ru(NPhtpy)_2](PF_6)_2$.[16] The distance between two amine sites may be too long compared to known organometallic bridges to mediate efficient amine−amine electronic coupling.[23]

The situation of the asymmetric complex $\mathbf{4}(PF_6)_2$ is more complex. Two chemically reversible anodic waves at +0.70 and +0.85 V are observed. Based on the above analysis on the symmetric complexes, these two waves are attributed to the $N^{\bullet+/0}$ process of the NPhtpy ligand and the $Os^{III/II}$ process. However, the order of these two processes needs further clarification (see below). The $N^{\bullet+/0}$ process of the Ntpy ligand is very likely embedded in the irreversible peak at +1.30 V. In the cathodic scan, all complexes show two redox waves attributed to the reduction behavior of the tpy ligands. The reduction potentials are comparable for both ruthenium and osmium series.

Spectroscopic Studies. The UV/vis absorption spectra of $\mathbf{1}(PF_6)_2$−$\mathbf{5}(PF_6)_2$ together with $[Os(tpy)_2](PF_6)_2$ are displayed in Figure 4a (see data in Table 1). When $\mathbf{1}(PF_6)_2$−$\mathbf{5}(PF_6)_2$ are substituted with amine groups, the molar absorptivities in the visible region are distinctly enhanced with respect to those of $[Os(tpy)_2](PF_6)_2$. These osmium complexes typically display both singlet and triplet metal-to-ligand charge-transfer transitions (^{1}MLCT around 450−600 nm; ^{3}MLCT around 600−800 nm). The ^{1}MLCT absorption maxima of $\mathbf{1}(PF_6)_2$−$\mathbf{5}(PF_6)_2$ are at 502, 518, 502, 516, and 515 nm, respectively, which are around 26 nm (for complexes $\mathbf{1}(PF_6)_2$ and $\mathbf{3}(PF_6)_2$ with one amine substituent) or 40 nm (for complexes $\mathbf{2}(PF_6)_2$, $\mathbf{4}(PF_6)_2$, and $\mathbf{5}(PF_6)_2$ with two amine substituents) red-shifted with respect to that of $[Os(tpy)_2](PF_6)_2$ (476 nm). The ^{1}MLCT absorptions of $\mathbf{1}(PF_6)_2$−$\mathbf{5}(PF_6)_2$ have very similar absorptivities and energies with respect to those of corresponding ruthenium analogues (Figure S2). TDDFT results suggest that the visible absorptions of the amine-containing complexes have significant contributions from the intraligand charge-transfer (ILCT) transitions (Figures S3−S8 and Table S1). Similar TDDFT results have previously been obtained for ruthenium analogues.[16]

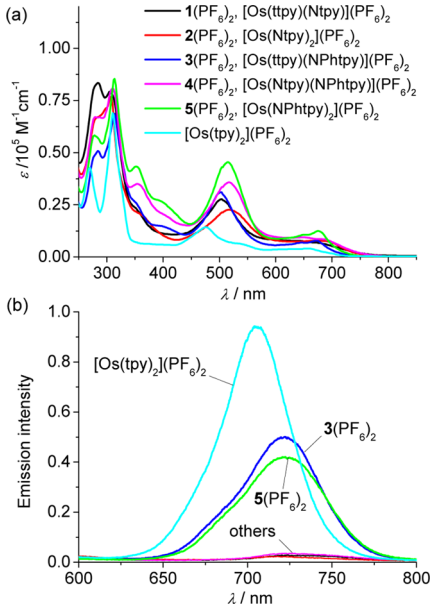

Figure 4. Electronic absorption spectra (a) and emission spectra (b) of $\mathbf{1}(PF_6)_2$−$\mathbf{5}(PF_6)_2$ and $[Os(tpy)_2](PF_6)_2$ in CH_3CN. The excitation wavelength is 480 nm for the emission spectra.

Figure 4b shows the emission spectra of these complexes in diluted CH_3CN at room temperature. Complexes $\mathbf{3}(PF_6)_2$ and $\mathbf{5}(PF_6)_2$ substituted with NPhtpy show distinct emission at 720 nm when excited at 480 nm, which is 15 nm red-shifted with respect to that of $[Os(tpy)_2](PF_6)_2$. The emission quantum yields of $\mathbf{3}(PF_6)_2$ and $\mathbf{5}(PF_6)_2$ is around 0.3−0.5% for both compounds using $[Os(tpy)_2](PF_6)_2$ as the reference standard (Φ = 1.4%).[21a] In contrast, complexes $\mathbf{1}(PF_6)_2$, $\mathbf{2}(PF_6)_2$, and $\mathbf{4}(PF_6)_2$ with Ntpy ligands show barely detectable emissions. Similar results were obtained by excitation at 650 nm (Figure S9a). Excitations at the ^{1}MLCT and ^{3}MLCT absorptions lead to emissions with the same energies. This is also supported by the excitation spectra of $\mathbf{3}(PF_6)_2$ and $\mathbf{5}(PF_6)_2$ (Figure S9b).

To further probe the electronic nature of the above osmium complexes, stepwise oxidative electrolysis were carried out at a transparent indium−tin−oxide (ITO) glass electrode. The absorption spectral changes from the visible to near-infrared (NIR) region were monitored by a UV/vis/NIR spectrometer.

Figure 5a,b shows the absorption changes of $\mathbf{1}(PF_6)_2$ upon one-electron (single) and the second one-electron (double) oxidations, respectively. In the single oxidation step (potential was increased from +0.4 to +1.0 V), the MLCT transitions significantly decreased and new NIR absorptions around 1000

DOI: 10.1021/acs.inorgchem.5b01420
Inorg. Chem. 2015, 54, 8136−8147

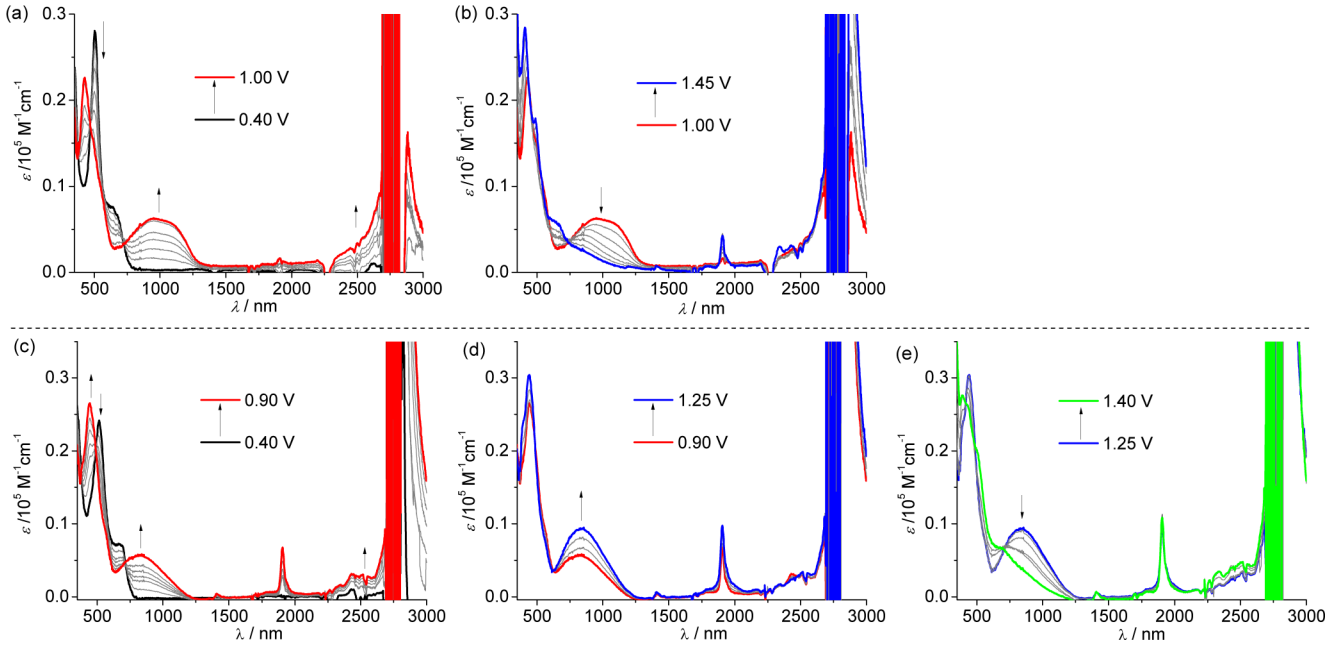

Figure 5. Absorption spectral changes of $\mathbf{1}(PF_6)_2$ (a,b) and $\mathbf{2}(PF_6)_2$ (c–e) upon single (a,c), double (b,d), and triple oxidation (e) by stepwise electrolysis at ITO glass in 0.1 M Bu_4NClO_4/CH_3CN. The applied potentials are referenced vs Ag/AgCl. The sharp peaks at around 1900 nm are from the solvent background.

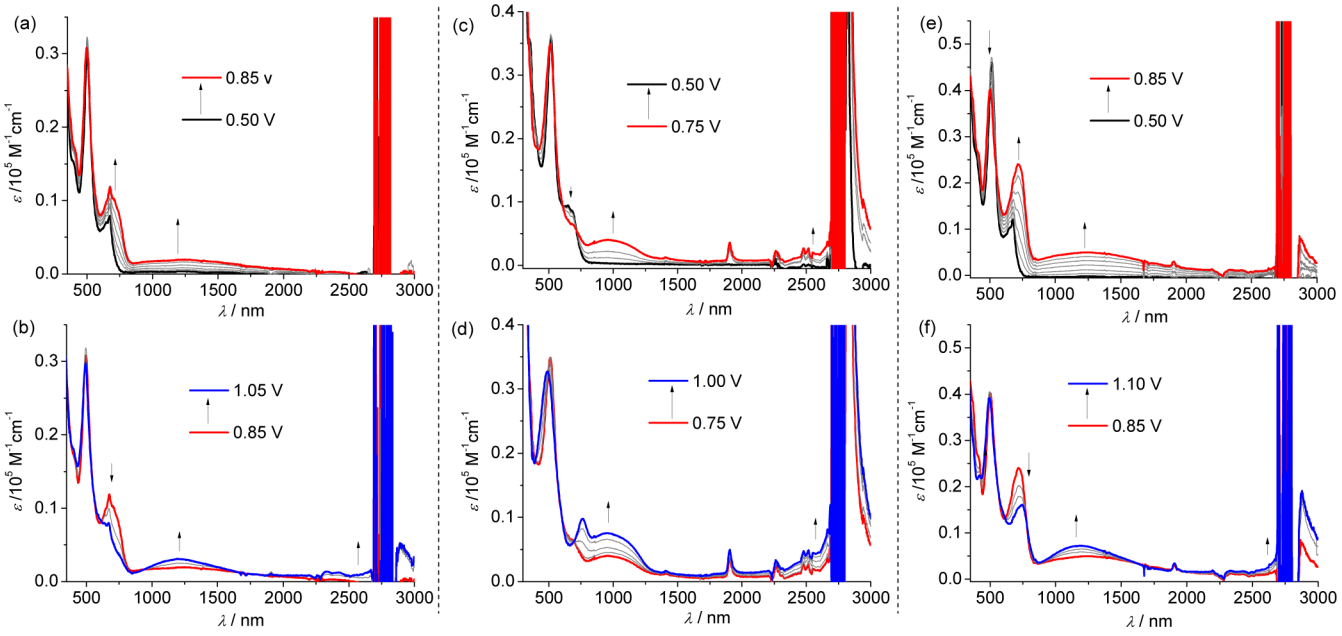

Figure 6. Absorption spectral changes of $\mathbf{3}(PF_6)_2$ (a,b), $\mathbf{4}(PF_6)_2$ (c,d), and $\mathbf{5}(PF_6)_2$ (e,f) upon stepwise electrolysis at ITO glass in 0.1 M Bu_4NClO_4/CH_3CN. The applied potentials are referenced vs Ag/AgCl.

nm appeared. At the same time, some absorptions between 2200 and 3000 nm appeared. Although these absorptions are heavily disturbed by the background noise, the increasing trend is very clear. These absorptions are characteristic of d-d transitions of Os^{III} complexes.[15,24] In the double oxidation step, the transitions at 1000 nm decreased and the Os^{III} d-d transitions remained unchanged. These results suggest that the single oxidation of $\mathbf{1}(PF_6)_2$ is largely associated with the $Os^{III/II}$ process. The absorption at 1000 nm of $\mathbf{1}^{3+}$ could be caused by the ligand-to-metal charge-transfer (LMCT) transitions from the amine unit (Ntpy ligand) to the oxidized Os ion, namely the N → Os^{III} CT transition.

The spectral changes of $\mathbf{2}(PF_6)_2$ upon single oxidation is quite similar to those of $\mathbf{1}(PF_6)_2$ (Figure 5c), again suggesting that the oxidation is largely associated with the osmium component. In the double oxidation step, the transitions around 800 nm continued to increase, which decreased upon the further increasing the potential (Figure 5d,e). In this step, it would be natural to consider that one amine site of $\mathbf{2}^{3+}$ was oxidized to give $\mathbf{2}^{4+}$, which will have the form of a mixed-valent bis-amine, [$N^{\bullet+}$-Os(III)-N], bridged by a osmium(III) component. However, the following theoretical calculations suggest that $\mathbf{2}^{4+}$ may also has the electronic structure as [$N^{\bullet+}$-Os(II)-$N^{\bullet+}$] and the absorptions at 800 nm could not be

DOI: 10.1021/acs.inorgchem.5b01420
Inorg. Chem. 2015, 54, 8136–8147

interpreted as IVCT transitions. This explanation is also consistent with the further growth of the band at 800 on further oxidation, as there are now two acceptor sites present in the same molecule.

When complexes $\mathbf{3}(PF_6)_2$ was subjected to the similar oxidative electrolysis, a much broader albeit weaker NIR absorption (relative to the absorption at 1000 nm of $\mathbf{1}^{3+}$) spanning from 800 to 2500 nm appeared in the first one-electron (1e) oxidation step (Figure 6a). According to the above electrochemical analysis, the single oxidation of $\mathbf{3}(PF_6)_2$ is mainly associated with the oxidation of the amine unit of the NPhtpy ligand. The increase of the absorption at around 750 nm is attributed to the $N^{\bullet+}$-localized transitions[20] and the NIR absorption of $\mathbf{3}^{3+}$ has the Os(II) → $N^{\bullet+}$ MLCT character. In the double oxidation step (Figure 6b), the NIR absorption continued to increase and the Os^{III} d-d marker transitions between 2200 and 3000 nm appeared. These spectral features are consistent with the above electrochemical assignments. The spectral changes of $\mathbf{5}(PF_6)_2$ (Figure 6e,f) are similar to those of $\mathbf{3}(PF_6)_2$. However, the molar absorptivity of the NIR band of $\mathbf{5}^{4+}$ (obtained from the two-electron (2e) oxidation of $\mathbf{5}(PF_6)_2$) doubles relative to that of $\mathbf{3}^{3+}$, consistent with the oxidations of two amine sites of $\mathbf{5}(PF_6)_2$. No IVCT transition can be distinguished during the single oxidation step. It should be mentioned that, despite to the absence of a potential splitting, the 1e-oxidized form $\mathbf{5}^{3+}$ is also present in equilibrium with the neutral ($\mathbf{5}^{2+}$) and 2e-oxidized form ($\mathbf{5}^{4+}$) at intermediate stages. If an IVCT transition is present, some peculiar spectroscopic profile could be detected.

The spectral changes of the asymmetric diamine complex $\mathbf{4}(PF_6)_2$ are somewhat different from those of other four complexes. In the first and second 1e oxidation steps, a new absorption band at around 1000 nm increased continuously. The appearance of the peak at 750 nm can be clearly assigned to the $N^{\bullet+}$-localized transition.[20] It seems that the Os^{III} d-d marker transitions between 2200 and 3000 nm continued to increase in both steps, although they are heavily overlapped with the solvent background. This may suggest that these two processes cannot be simply assigned to either a $Os^{III/II}$ or $N^{\bullet+/0}$ process. Both osmium and amine components could be oxidized in the single and double oxidation, respectively, and both $\mathbf{4}^{3+}$ and $\mathbf{4}^{4+}$ have rather delocalized charge.

DFT and TDDFT Studies. The TDDFT results of $\mathbf{1}^{2+}$–$\mathbf{5}^{2+}$ are presented in Figures S3–S8. We focus the DFT and TDDFT results on the singly or doubly oxidized states. These calculations were performed on the level of theory of B3LYP/LANL2DZ/6-31G*/CPCM (see details in the Experimental Section). Figure 7 shows the Mulliken spin density distributions ($\alpha - \beta$) of $\mathbf{1}^{3+}$–$\mathbf{5}^{3+}$ and $\mathbf{2}^{4+}$ and $\mathbf{4}^{4+}$ in the triplet state. The singlet state of $\mathbf{2}^{4+}$ and of $\mathbf{4}^{4+}$ was calculated to be 0.48 and 0.53 eV higher in energy relative to the triplet state, respectively, suggesting that the ground state of $\mathbf{2}^{4+}$ and $\mathbf{4}^{4+}$ is the triplet state. The spin density of $\mathbf{1}^{3+}$ is distributed among the [Os(Ntpy)] component. However, the Os ion has larger contribution relative to the Ntpy ligand (0.629 vs 0.377), consistent with the above experimental results that the single oxidation of $\mathbf{1}(PF_6)_2$ is more biased toward the $Os^{III/II}$ process. The situation of $\mathbf{2}^{3+}$ is very similar to $\mathbf{1}^{3+}$. For the NPhtpy-containing complexes $\mathbf{3}^{3+}$, $\mathbf{4}^{3+}$, and $\mathbf{5}^{3+}$, the spin density mainly concentrates on the NPhtpy ligand. However, the osmium ion of $\mathbf{4}^{3+}$ makes slightly larger contribution (0.113) with respect to those of $\mathbf{3}^{3+}$ and $\mathbf{5}^{3+}$. This could explain, in the above spectroelectrochemical measurements, why the Os^{III} d-d marker transitions appeared in the single oxidation step of $\mathbf{4}(PF_6)_2$.

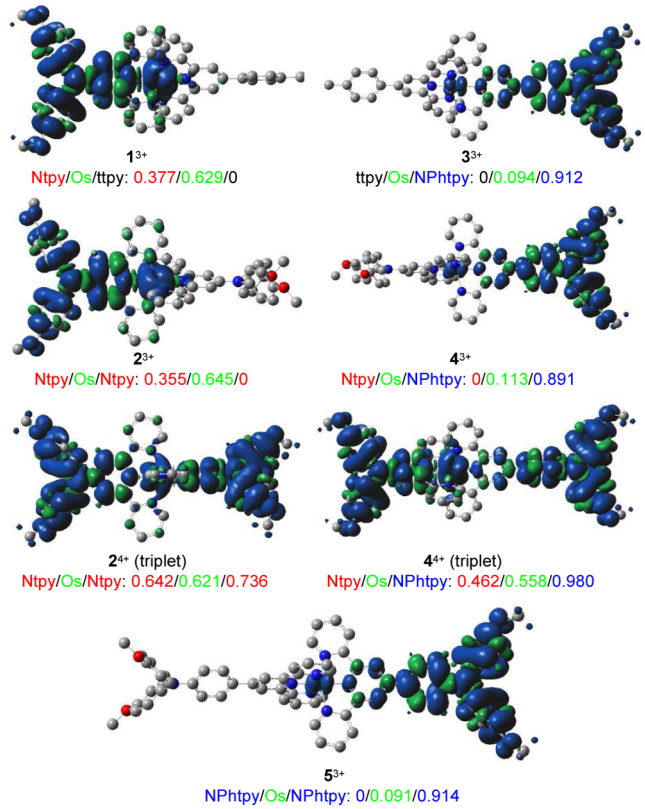

Figure 7. DFT-calculated spin density distributions.

The spin density distribution of triplet $\mathbf{2}^{4+}$ and $\mathbf{4}^{4+}$ are rather delocalized. The contribution of each segment is 0.642/0.621/0.736 for Ntpy/Os/Ntpy of $\mathbf{2}^{4+}$ and 0.462/0.558/0.980 for Ntpy/Os/NPhtpy of $\mathbf{4}^{4+}$, respectively. This suggests that $\mathbf{2}^{4+}$ and $\mathbf{4}^{4+}$ have resonance structures between [$N^{\bullet+}$-Os(III)-N] and [$N^{\bullet+}$-Os(II)-$N^{\bullet+}$]. It should be mentioned here that DFT methods often overestimate charge delocalization and these results should be taken with care.

TDDFT calculations have been carried out on $\mathbf{1}^{3+}$–$\mathbf{5}^{3+}$ and triplet $\mathbf{2}^{4+}$ and $\mathbf{4}^{4+}$. The predicted excitations of $\mathbf{2}^{3+}$, $\mathbf{2}^{4+}$, $\mathbf{4}^{3+}$, and $\mathbf{4}^{4+}$ are summarized in Figures 8 and 9 and Table 2. The NIR transitions of these complexes can be reproduced by TDDFT predications. However, the predicted excitations are slightly lower in energy relative to the experimentally observed data. The predicted D_3 excitation (λ = 1294 nm, f = 0.4695) of $\mathbf{2}^{3+}$ is mainly responsible for the observed for the NIR absorption band around 800 nm. This excitation is dominated by the β spin transition from the HOSO-1 (HOSO = highest occupied spin orbital) to the LUSO (LUSO = lowest unoccupied spin orbital). The segmental Mulliken contribution of Os/Ntpy is 0.17/0.79 for the HOSO-1 and 0.45/0.49 for the LUSO, respectively. This suggests the character of N → Os(III) LMCT transition as has been discussed in the above spectroelectrochemical results. The $N^{\bullet+}$-localized transitions can be reproduced by the predicted D_5 excitation (λ = 750 nm, f = 0.1394, β-HOSO-5 → β-LUSO). In the doubly oxidized state $\mathbf{2}^{4+}$, the NIR transition can be explained by the predicted T_3 excitation, which has the main character of MLCT transitions (dominated by β-HOSO-1 → β-LUSO and β-HOSO-2 → β-LUSO+1 transitions). Other predicted NIR excitations, e.g., T_1 and T_2, have negligible oscillator strengths

DOI: 10.1021/acs.inorgchem.5b01420
Inorg. Chem. 2015, 54, 8136–8147

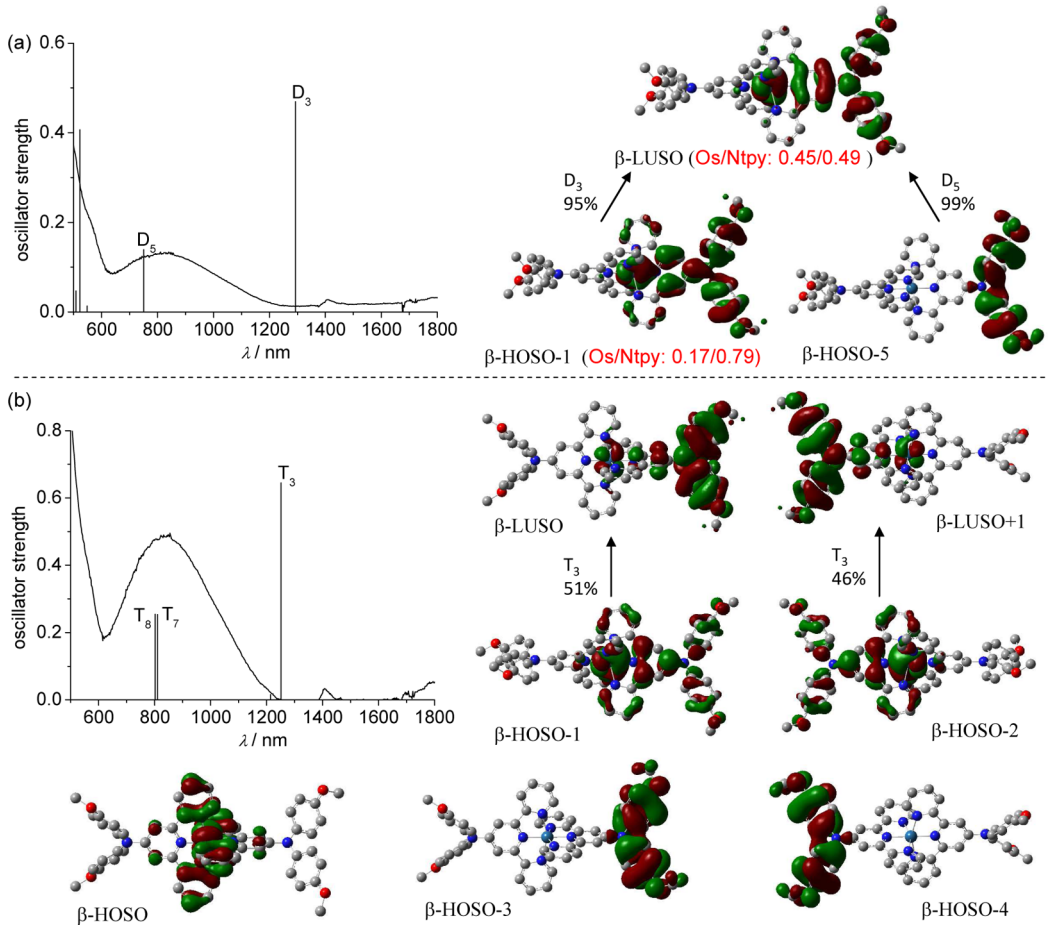

Figure 8. TDDFT-predicted excitations and involved spin orbitals of $\mathbf{2}^{3+}$ (a) and $\mathbf{2}^{4+}$ (b). The absorption spectra of $\mathbf{2}^{3+}$ and $\mathbf{2}^{4+}$ are included for comparison.

and also have MLCT characters. No IVCT transitions have been predicted. The T_7 and T_8 excitations around 800 nm with large oscillator strengths are attributed to the $N^{\bullet+}$-localized transitions.

For complex $\mathbf{4}^{3+}$, the predicted D_2 excitation (λ = 1189 nm, f = 0.2413) associated with the β-HOSO-2 → β-LUSO transition is mainly responsible for the NIR absorptions at 1000 nm, which has major contribution from Os(II) → $N_{NPhtpy}^{\bullet+}$ MLCT transitions. This again is consistent with the above spectroelectrochemical results. The predicted D_5 excitation (λ = 730 nm, f = 0.2775) with the β-HOSO-5 → β-LUSO is associated with the $N^{\bullet+}$-localized transitions. In the doubly oxidized state $\mathbf{4}^{4+}$, the predicted T_3 excitation (λ = 1300 nm, f = 0.4711) is responsible for the observed absorption at 1000 nm. This excitation is dominated by the β-HOSO → β-LUSO transition. On the basis of the segmental Mulliken contribution analysis of these two orbitals (Ntpy/Os: 0.71/0.24 for β-HOSO; 0.56/0.38 for β-LUSO), this transition has some Os → $N_{Ntpy}^{\bullet+}$ MLCT characters. On the other hand, the predicted T_6 excitation has the character of Os → $N_{NPhtpy}^{\bullet+}$ MLCT transitions (β-HOSO-2 → β-LUSO+1). The T_7 and T_8 excitations are associated with the $N^{\bullet+}$-localized transitions. Other predicted excitations have negligible oscillator strengths.

The TDDFT results of $\mathbf{1}^{3+}$ with one Ntpy ligand are very similar to those of $\mathbf{2}^{3+}$ with two Ntpy ligands. For the NPhtpy-containing complexes, the TDDFT results of $\mathbf{3}^{3+}$ and $\mathbf{5}^{3+}$ are very similar to those of $\mathbf{2}^{3+}$. These results are summarized in Figure S10 and Table S2. Since no amine−amine electronic coupling is present in complex **5**, the TDDFT results of $\mathbf{5}^{3+}$ should be eligible for the explanation of the obtained absorption of $\mathbf{5}^{4+}$ ($\mathbf{5}^{3+}$ and $\mathbf{5}^{4+}$ have the same absorption pattern albeit different absorptivities).

Electron Paramagnetic Resonace (EPR) Studies. The recording of EPR signals of osmium(III) complexes has been known notoriously difficult.[15] However, nitrogen-centered organic radicals should exhibit distinct EPR signals. This should allow us to differentiate the osmium- or nitrogen-centered spins. Complexes $\mathbf{3}^{3+}$ and $\mathbf{5}^{3+}$, which were obtained by the oxidation of $\mathbf{3}(PF_6)_2$ and $\mathbf{5}(PF_6)_2$ with 0.5 equiv of cerium ammonium nitrate (CAN), show distinct EPR signals at g = 2.00 in CH_3CN at room temperature (Figure 10). The use of 0.5 equiv of the oxidant, instead of 1 equiv, is for the purpose of preventing over-oxidaiton. In contrast, no EPR signals could be obtained for samples $\mathbf{1}^{3+}$, $\mathbf{2}^{3+}$, and $\mathbf{4}^{3+}$ prepared by the same method. This is in agreement with the above electrochemical and theoretical results, namely, the 1e oxidations of $\mathbf{3}(PF_6)_2$ and $\mathbf{5}(PF_6)_2$ are largely associated with the oxidation of the NPhtpy ligand. However, the oxidation of the osmium component makes great or dominant contribution to the 1e oxidations of the other three complexes.

CONCLUSION

In summary, five osmium bisterpyridine complexes with one or two redox-active amine substituents have been synthesized and studied. All complexes show stepwise oxidations of the osmium ion and the amine segment. However, the redox potential and

DOI: 10.1021/acs.inorgchem.5b01420
Inorg. Chem. 2015, 54, 8136−8147

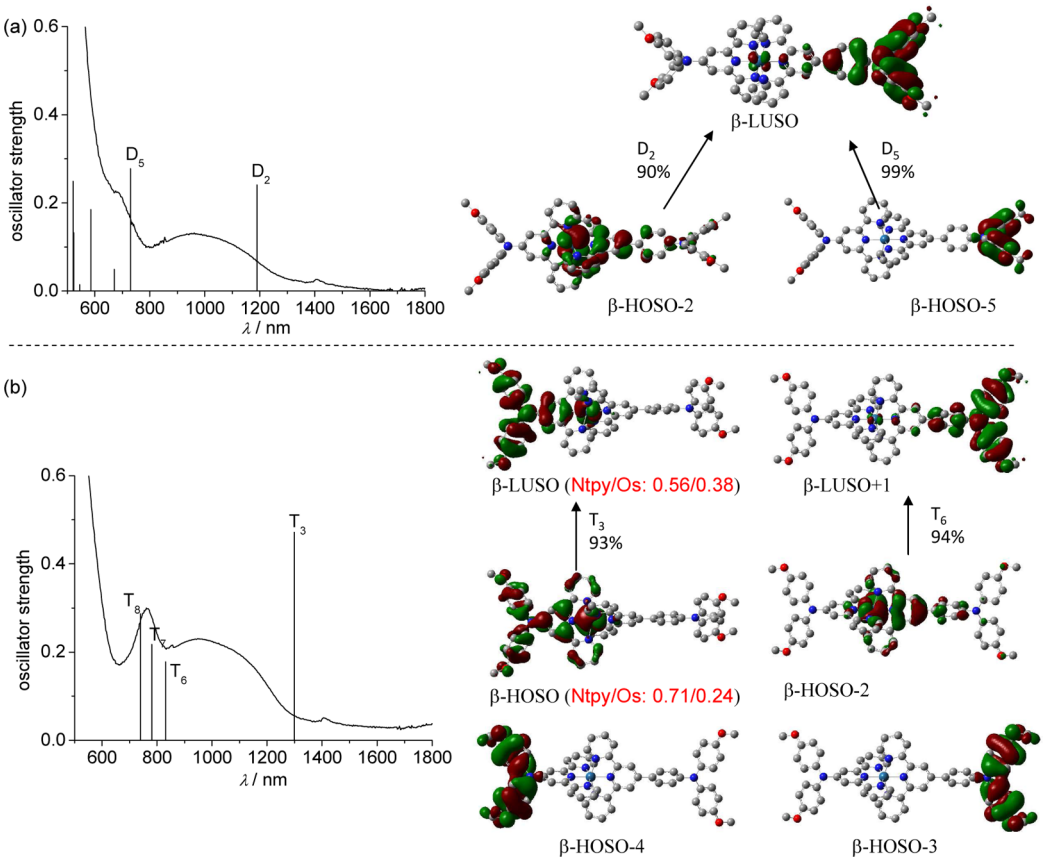

Figure 9. TDDFT-predicted excitations and involved spin orbitals of $\mathbf{4}^{3+}$ (a) and $\mathbf{4}^{4+}$ (b). The absorption spectra of $\mathbf{4}^{3+}$ and $\mathbf{4}^{4+}$ are included for comparison.

the order of the $Os^{III/II}$ and $N^{\bullet+/0}$ processes vary significantly depending on the electronic nature of the amine substituents. In the singly oxidized state, either Os(II) → $N^{\bullet+}$ MLCT or N → Os(III) LMCT transitions in the NIR region are observed. This work shows that the electrochemical and photophysical properties of osmium complexes can be significantly modulated by the presence of additional redox-active motifs.

For all of the three complexes with two amine substituents, no evidence has been observed for presence of the osmium-mediated amine−amine electronic coupling. For complex $\mathbf{2}(PF_6)_2$ with two Ntpy ligands, the single-oxidation step is mainly associated with the $Os^{III/II}$ process. In the doubly oxidized state, the complex has a big contribution from the $[N^{\bullet+}\text{-}Os(II)\text{-}N^{\bullet+}]$ electronic structure and the observed NIR absorptions mainly have the character of Os(II) → $N_{Ntpy}^{\bullet+}$ MLCT transitions. For the asymmetric complex $\mathbf{4}(PF_6)_2$ with one Ntpy and one NPhtpy ligand, the single-oxidation step is mainly associated with the $N_{NPhtpy}^{\bullet+}$ process. The NIR absorptions are dominated by the Os(II) → $N_{NPhtpy}^{\bullet+}$ MLCT transitions. For the complex $\mathbf{5}(PF_6)_2$ with two NPhtpy ligands, the amine−amine distance is too long for efficient electronic coupling.

Some distinct differences are present between these osmium complexes and the previously reported ruthenium analogues.[16,17] The lower Os(III/II) potential relative to the Ru(III/II) potential completely changes the electronic structure and the nature of the charge-transfer transitions of the [M(Ntpy)]-type complexes in the one-electron-oxidized form. In addition, the similarity between the Os(III/II) potential and the $N_{Ntpy}^{\bullet+/0}$ potential results in the stronger metal−ligand electronic coupling with respect to the ruthenium analogue. These suggest that the potential difference between/among involved redox processes makes critical roles in determining the electron nature and the degree of electronic coupling of molecular materials with multiple redox-active components.

EXPERIMENTAL SECTION

Synthesis. NMR spectra were recorded in the designated solvent on a Bruker Avance 300 or 400 MHz spectrometer. Spectra are reported in ppm values from residual protons of deuterated solvent. Mass data were obtained with a Bruker Daltonics Inc. (Germany) Autoflex III MALDI-TOF mass spectrometer. The matrix for MALDI-TOF measurement was α-cyano-4-hydroxycinnamic acid. Microanalysis was carried out using a Thermo Scientific (USA) Flash EA 1112 analyzer at the Institute of Chemistry, Chinese Academy of Sciences.

Synthesis of [Os(ttpy)Cl₃] and [Os(NPhtpy)Cl₃]. According to the known procedure,[15g,25] these two complexes were prepared by heating the mixture of ttpy or NPhtpy (0.1 mmol) with $[(NH_4)_2OsCl_6]$ (0.1 mmol) in ethylene glycol (5 mL) at 160 °C for 1 h. The precipitate formed during the reaction was filtered and washed with ethanol, water and diethyl ether successively (80−90% yield). The obtained samples were used for next transformation without further characterization and purification.

Synthesis of Complex $\mathbf{1}(PF_6)_2$, *[Os(ttpy)(Ntpy)]*$(PF_6)_2$. A suspension of $[(ttpy)OsCl_3]$ (31.0 mg, 0.050 mmol) and ligand Ntpy (23.0 mg, 0.050 mmol) was refluxed in 5 mL of ethylene glycol under nitrogen atmosphere for 2 h. After cooling to room temperature, 5 mL of saturated aqueous KPF_6 solution was added for the anion exchange. After filtration and washing successively with water and ether, the obtained solid was subjected to column chromatography on silica gel (eluent: CH_3CN/H_2O/saturated aqueous KNO_3, 30/1/0.05), fol-

DOI: 10.1021/acs.inorgchem.5b01420
Inorg. Chem. 2015, 54, 8136−8147

Table 2. TDDFT-Predicted Excitations of 2^{3+}, 2^{4+}, 4^{3+}, and 4^{4+} [a]

complex		λ/nm	f	dominant transitions (percent contribution)
2^{3+}	D_1	3426	0	β-HOSO → β-LUSO (69%); β-HOSO-3 → β-LUSO (26%)
	D_2	2172	0.0005	β-HOSO-2 → β-LUSO (95%)
	D_3	1294	0.4695	β-HOSO-1 → β-LUSO (95%)
	D_4	1104	0.0003	β-HOSO-3 → β-LUSO (64%); β-HOSO → β-LUSO (31%)
	D_5	750	0.1394	β-HOSO-5 → β-LUSO (99%)
2^{4+}	T_1	1380	0.0004	β-HOSO → β-LUSO (97%)
	T_2	1357	0.0004	β-HOSO → β-LUSO+1 (97%)
	T_3	1251	0.6443	β-HOSO-2 → β-LUSO+1 (46%); β-HOSO-1 → β-LUSO (51%)
	T_4	1214	0.0157	β-HOSO-2 → β-LUSO (78%)
	T_5	1193	0.0005	β-HOSO-1 → β-LUSO+1 (79%)
	T_6	1058	0.0004	β-HOSO-2 → β-LUSO+1 (48%); β-HOSO-1 → β-LUSO (43%)
	T_7	810	0.2539	β-HOSO-3 → β-LUSO (99%)
	T_8	802	0.2544	β-HOSO-4 → β-LUSO+1 (99%)
4^{3+}	D_1	1179	0.0009	β-HOSO → β-LUSO (98%)
	D_2	1189	0.2413	β-HOSO-2 → β-LUSO (90%)
	D_3	1181	0.0045	β-HOSO-1 → β-LUSO (92%)
	D_4	891	0	β-HOSO-3 → β-LUSO (96%)
	D_5	730	0.2775	β-HOSO-5 → β-LUSO (99%)
4^{4+}	T_1	1680	0.0003	β-HOSO-1 → β-LUSO (96%)
	T_2	1446	0.0004	β-HOSO-2 → β-LUSO (95%)
	T_3	1300	0.4711	β-HOSO → β-LUSO (93%)
	T_4	865	0.0003	β-HOSO → β-LUSO+1 (99%)
	T_5	853	0	β-HOSO-1 → β-LUSO+1 (98%)
	T_6	831	0.1778	β-HOSO-2 → β-LUSO+1 (94%)
	T_7	781	0.2179	β-HOSO-4 → β-LUSO (99%)
	T_8	739	0.2863	β-HOSO-3 → β-LUSO+1 (98%)

[a]Computed at the TDDFT/UB3LYP/LANL2DZ/6-31G*/CPCM level of theory. *D* = doublet; *T* = triplet; *f* = oscillator strength; HOSO = highest occupied spin orbital; LUSO = lowest unoccupied spin orbital.

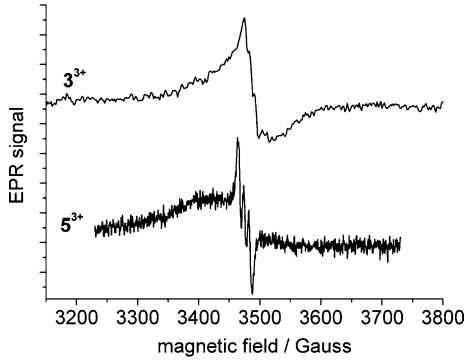

Figure 10. EPR signals of 3^{3+} (up) and 5^{3+} (bottom) in CH_3CN at room temperature.

lowed by anion exchange using KPF_6, to afford 48.2 mg of $\mathbf{1}(PF_6)_2$ as a purple solid in 76% yield. ^{1}H NMR (acetone-d_6, 300 MHz): δ 9.36 (s, 2H), 9.00 (d, *J* = 8.4 Hz, 2H), 8.41 (d, *J* = 8.1 Hz, 2H), 8.32 (s, 2H), 8.19 (d, *J* = 8.4 Hz, 2H), 7.96 (t, *J* = 7.2 Hz, 2H), 7.75−7.85 (m, 4H), 7.50−7.60 (m, 8H), 7.34 (t, *J* = 7.2 Hz, 2H), 7.10−7.20 (m, 6H), 3.90 (s, 6H), 2.54 (s, 3H). ^{13}C NMR (acetone-d_6, 75 M): δ 161.03, 160.37, 158.59, 156.58, 155.78, 154.85, 152.49, 152.44, 146.07, 140.56, 137.52, 137,47, 137.29, 133.31, 129.92, 128.55, 128.04, 127.79, 127.73, 124.63, 124.50, 119.47, 115.59, 108.90, 55.04, 20.32. MALDI-TOF MS (*m*/*z*): 1120.5 for $[M - PF_6]^+$, 975.5 for $[M - 2PF_6]^+$. Anal. Calcd for $C_{51}H_{41}F_{12}N_7O_2OsP_2 \cdot 4H_2O$: C, 45.84; H, 3.70; N, 7.34. Found: C, 45.76; H, 3.29, N, 7.16.

Synthesis of Complex $\mathbf{2}(PF_6)_2$, *[Os(Ntpy)$_2$](PF$_6$)$_2$*. A suspension of ligand Ntpy (46.0 mg, 0.10 mmol) and $[(NH_4)_2OsCl_6]$ (22.0 mg, 0.050 mmol) was refluxed in 5 mL of ethylene glycol under nitrogen atmosphere for 2 h. After cooling to room temperature, 5 mL of saturated aqueous KPF_6 solution was added for the anion exchange. After filtration and washing successively with water and ether, the obtained solid was subjected to column chromatography on silica gel. (eluent: CH_3CN/H_2O/saturated aqueous KNO_3, 30/1/0.05), followed by anion exchange using KPF_6, to afford 49.0 mg of $\mathbf{2}(PF_6)_2$ as a purple solid in 70% yield. ^{1}H NMR (acetone-d_6, 400 MHz): δ 8.39 (d, *J* = 8.4 Hz, 4H), 8.29 (s, 4H), 7.77 (t, *J* = 7.2 Hz, 4H), 7.63 (d, *J* = 5.6 Hz, 4H), 7.48 (d, *J* = 8.8 Hz, 8H), 7.20 (t, *J* = 6.4 Hz, 4H), 7.14 (d, *J* = 8.8 Hz, 8 H), 3.90 (s, 12H). ^{13}C NMR (acetone-d_6, 75 M): δ 160.95, 158.44, 156.00, 155.01, 152.33, 137.49, 137.04, 128.42, 127.83, 124.30, 115.54, 108.86, 55.03. MALDI-TOF MS (*m*/*z*): 1257.1 for $[M - PF_6]^+$, 1112.1 for $[M - 2PF_6]^+$. Anal. Calcd for $C_{58}H_{48}F_{12}N_8O_4OsP_2 \cdot 2H_2O$: C, 48.47; H, 3.65; N, 7.80. Found: C, 48.29; H, 3.65, N, 7.80.

Synthesis of Complex $\mathbf{3}(PF_6)_2$, *[Os(ttpy)(NPhtpy)](PF$_6$)$_2$*. This complex was prepared similarly as $\mathbf{1}(PF_6)_2$ from the reaction of $[(ttpy)OsCl_3]$ with NPhtpy (0.05 mmol scale, purple solid, 68% yield). ^{1}H NMR (acetone-d_6, 300 MHz): δ 9.41 (s, 2H), 9.34 (s, 2H), 8.95−9.05 (m, 4H), 8.20 (d, *J* = 8.1 Hz, 2H), 8.11 (d, *J* = 9.0 Hz, 2H), 7.88−7.98 (m, 4H), 7.65−7.70 (m, 4H), 7.56 (d, *J* = 8.1 Hz, 2H), 7.18−7.30 (m, 8H), 7.08 (d, *J* = 8.4 Hz, 2H), 7.02 (d, J = 9.0 Hz, 4H), 3.84 (s, 6H), 2.54 (s, 3H). ^{13}C NMR (acetone-d_6, 75 M): δ 160.48, 157.17, 155.59, 155.23, 152.56, 152.53, 151.19, 147.59, 147.29, 140.73, 139.70, 137.84, 133.15, 129.94, 128.87, 127.97, 127.92, 127.88, 127.64, 126.37, 124.89, 124.79, 119.68, 118.80, 118.59, 115.02, 54.96, 20.35. MALDI-TOF MS (*m*/*z*): 1196.1 for $[M - PF_6]^+$, 1051.1 for $[M - 2PF_6]^+$. Anal. Calcd for $C_{57}H_{45}F_{12}N_7O_2OsP_2 \cdot 2H_2O$: C, 49.75; H, 3.59; N, 7.12. Found: C, 49.35; H, 3.47, N, 7.10.

Synthesis of Complex $\mathbf{4}(PF_6)_2$, *[Os(Ntpy)(NPhtpy)](PF$_6$)$_2$*. This complex was prepared similarly as $\mathbf{1}(PF_6)_2$ from the reaction of Ntpy

DOI: 10.1021/acs.inorgchem.5b01420
Inorg. Chem. 2015, 54, 8136−8147

with [(NPhtpy)$OsCl_3$] (0.05 mmol scale, purple solid, 78% yield). ^{1}H NMR (acetone-d_6, 300 MHz): δ 9.29 (s, 2H), 8.97 (d, J = 8.1 Hz, 2H), 8.43 (d, J = 8.4 Hz, 2H), 8.33 (s, 2H), 8.08 (d, J = 9.0 Hz, 2H), 7.95 (t, J = 7.5 Hz, 2H), 7.70−7.80 (m, 4H), 7.45−7.60 (m, 6H), 7.32 (t, J = 7.2 Hz, 2H), 7.10−7.25 (m, 10H), 7.10 (d, J = 9.0 Hz, 2H), 7.05 (d, J = 9.0 Hz, 4H), 3.90 (s, 6H), 3.85 (s, 6H). ^{13}C NMR (acetone-d_6, 75 M): δ 161.10, 160.45, 158.56, 157.12, 156.36, 155.68, 154.98, 152.42, 151.00, 146.21, 139.75, 137.45, 137.39, 137.33, 128.73, 128.56, 127.96, 127.74, 127.56, 126.65, 124.47, 118.70, 118.60, 115.58, 114.99, 108.88. MALDI-TOF MS (m/z): 1332.8 for $[M - PF_6]^+$, 1187.9 for $[M - 2PF_6]^+$. Anal. Calcd for $C_{64}H_{52}F_{12}N_8O_4OsP_2 \cdot 3H_2O$: C, 50.20; H, 3.82; N, 7.32; Found: C, 50.08; H, 3.54; N, 7.47.

Synthesis of Complex $\mathbf{5}(PF_6)_2$, *[Os(NPhtpy)$_2$](PF$_6$)$_2$.* This complex was prepared similarly as $\mathbf{2}(PF_6)_2$ from the reaction of $[(NH_4)_2OsCl_6]$ with two equiv NPhtpy (0.05 mmol scale, purple solid, 91% yield). ^{1}H NMR (acetone-d_6, 300 MHz): δ 9.35 (s, 4H), 8.99 (d, J = 6.0 Hz, 4H), 8.10 (d, J = 6.0 Hz, 4H), 7.94 (t, J = 6.0 Hz, 4H), 7.68 (d, J = 3.0 Hz, 4H), 7.15−7.30 (m, 12H), 7.10 (d, J = 9.0 Hz, 4H), 7.03 (d, J = 6.0 Hz, 8H), 3.85 (s, 12H). ^{13}C NMR (acetone-d_6, 75 M): δ 160.60, 157.20, 155.39, 152.51, 151.21, 147.43, 139.68, 137.79, 128.83, 127.88, 127.62, 126.36, 124.74, 118.60, 115.02, 54.95. MALDI-TOF MS (m/z): 1408.8 for $[M - PF_6]^+$, 1263.9 for $[M - 2PF_6]^+$. Anal. Calcd for $C_{70}H_{56}F_{12}N_8O_4OsP_2 \cdot 2H_2O$: C, 52.90; H, 3.80; N, 7.05; Found: C, 53.21; H, 3.61; N, 7.31.

X-ray Crystallography. The X-ray diffraction data were collected using a Rigaku Saturn 724 diffractometer on a rotating anode (Mo K radiation, 0.71073 Å) at 173 K. The structure was solved by the direct method using SHELXS-97[26] and refined with Olex2.[27] The structure graphics were generated using Olex2.

Crystallographic data for $\mathbf{2}(PF_6)_2$ (CCDC no. 1055941): $C_{58}H_{48}F_{12}N_8O_4OsP_2$, M = 1401.18, triclinic, space group $P\bar{1}$, a = 9.0219(18), b = 16.256(3), and c = 22.750(4) Å, α = 110.71(3)°, β = 97.09(3)°, γ = 93.99(3)°, U = 3073.9(12) Å^3, T = 173 K, Z = 2, 12 468 reflections measured, radiation type Mo Kα, radiation wavelength 0.71073 Å, final R indices $R1$ = 0.0804, w$R2$ = 0.2086, R indices (all data) $R1$ = 0.0819, w$R2$ = 0.2107.

Crystallographic data for $\mathbf{4}(PF_6)_2$ (CCDC no. 1055940): $C_{64}H_{52}F_{12}N_8O_4OsP_2$, M = 1477.27, monoclinic, space group $C12/c1$, a = 36.792(10), b = 16.180(4), and c = 22.067(6) Å, α = 90°, β = 95.302(4)°, γ = 90°, U = 13080(6) Å^3, T = 173 K, Z = 8, 42 450 reflections measured, radiation type Mo Kα, radiation wavelength 0.71073 Å, final R indices $R1$ = 0.1040, w$R2$ = 0.1993, R indices (all data) $R1$ = 0.1247, w$R2$ = 0.2113.

Spectroscopic Measurement. Absorption spectra were recorded on a PerkinElmer Lambda 750 UV/vis/NIR spectrophotometer at room temperature. Spectroelectrochemical measurements were performed in a thin layer cell (optical length: 0.2 cm), in which a transparent ITO glass electrode (<10 Ω/square) was set in the indicated solvent that contained the compound to be studied (about 5 × 10^{-5} M) and 0.1 M Bu_4NClO_4 as the supporting electrolyte. A platinum wire and Ag/AgCl in saturated aqueous NaCl was used as the counter electrode and reference electrode, respectively. The cell was put into the spectrometer to monitor the spectral change during electrolysis.

Electrochemical Measurement. All electrochemical measurements were taken using a CH Instruments (USA) 660D potentiostat with one-compartment electrochemical cell under an atmosphere of nitrogen. All measurements were carried out in CH_3CN containing 0.1 M $^n Bu_4NClO_4$ as the supporting electrolyte at a scan rate of 100 mV/s (for cyclic voltammetry). The working electrode was a Pt disk electrode. The electrode was polished prior to use with 0.05 μm alumina and rinsed thoroughly with water and acetone. A large area platinum wire coil was used as the counter electrode. All potentials are referenced to Ag/AgCl electrode in saturated aqueous NaCl without regard for the liquid junction potential. Potentials vs ferrocene$^{+/0}$ can be deduced by subtracting 0.45 V.

Computational Methods. DFT and TDDFT calculations are carried out using the B3LYP[28] exchange correlation functional implemented in the Gaussian 09 program package.[29] The electronic structures of complexes were determined using a general basis set with the Los Alamos effective core potential LanL2DZ basis set for osmium, and 6-31G* for other atoms.[30] No symmetry constraints were used in the optimization (nosymm keyword was used). Solvent effects (CH_3CN) are included in all calculations with the conductor-like polarizable continuum model (CPCM).[31] Frequency calculations have been performed with the same level of theory to ensure the optimized geometries to be local minima. All orbitals have been computed at an isovalue of 0.02 e/bohr^3. The TDDFT-predicted spectra were generated using GaussView 5.0.

EPR Measurements. EPR Measurements were performed on a Bruker ELEXSYS E500-10/12 spectrometer at room temperature in CH_3CN. The spectrometer frequency ν was 9.75 × 10^9 Hz. The mono-oxidized forms $\mathbf{1}^{3+}$−$\mathbf{5}^{3+}$ were obtained by adding 0.5 equiv of CAN to $\mathbf{1}(PF_6)_2$−$\mathbf{5}(PF_6)_2$ in CH_3CN in an NMR tube, and these samples were directly used for EPR measurements.

■ ASSOCIATED CONTENT

Supporting Information

The Supporting Information is available free of charge on the ACS Publications website at DOI: 10.1021/acs.inorgchem.5b01420.

CVs of Ntpy and NPhtpy; comparison of the absorption spectra of Ru and Os series compounds; TDDFT results of $\mathbf{1}^{2+}$−$\mathbf{5}^{2+}$, $\mathbf{1}^{3+}$, $\mathbf{3}^{3+}$, and $\mathbf{5}^{3+}$; emission spectra excited at 650 nm of $\mathbf{1}(PF_6)_2$−$\mathbf{5}(PF_6)_2$ and $[Os(tpy)_2](PF_6)_2$ and excitation spectra of $\mathbf{3}(PF_6)_2$, $\mathbf{5}(PF_6)_2$, and $[Os(tpy)_2](PF_6)_2$; and NMR and mass spectra of new compounds (PDF)

Cartesian coordinates of DFT-optimized structures (XYZ)

X-ray crystallographic data of $\mathbf{2}(PF_6)_2$ (CIF)

X-ray crystallographic data of $\mathbf{4}(PF_6)_2$ (CIF)

■ AUTHOR INFORMATION

Corresponding Authors

*E-mail: shaojiangyang@iccas.ac.cn (J.-Y.S.).

*E-mail: zhongyuwu@iccas.ac.cn (Y.-W.Z.).

*E-mail: jnyao@iccas.ac.cn (J.Y.).

Notes

The authors declare no competing financial interest.

■ ACKNOWLEDGMENTS

We thank the National Natural Science Foundation of China (grants 91227104, 21271176, 21472196, and 21221002), the National Basic Research 973 program of China (grant 2011CB932301), the Ministry of Science and Technology of China (grant 2012YQ120060), and the Strategic Priority Research Program of the Chinese Academy of Sciences (grant XDB 12010400) for funding support.

■ REFERENCES

(1) (a) Launay, J.-P. *Coord. Chem. Rev.* **2013**, *257*, 1544. (b) Sakamoto, R.; Katagiri, S.; Maeda, H.; Nishihara, H. *Coord. Chem. Rev.* **2013**, *257*, 1493.

(2) (a) Kaim, W. *Coord. Chem. Rev.* **2011**, *255*, 2503. (b) Deibel, N.; Hohloch, S.; Sommer, M. G.; Schweinfurth, D.; Ehret, F.; Braunstein, P.; Sarkar, B. *Organometallics* **2013**, *32*, 7366. (c) Cui, B.-B.; Yao, C.-J.; Yao, J.; Zhong, Y.-W. *Chem. Sci.* **2014**, *5*, 932. (d) Das, H. S.; Schweinfurth, D.; Fiedler, J.; Khusniyarov, M. M.; Mobin, S. M.; Sarkar, B. *Chem. - Eur. J.* **2014**, *20*, 4334.

(3) (a) Simao, C.; Mas-Torrent, M.; Crivillers, N.; Lloveras, V.; Artes, J. M.; Gorostiza, P.; Veciana, J.; Rovira, C. *Nat. Chem.* **2011**, *3*, 359. (b) Terada, K.; Kanaizuka, K.; Iyer, V. M.; Sannodo, M.; Saito, S.; Kobayashi, K.; Haga, M.-a. *Angew. Chem., Int. Ed.* **2011**, *50*, 6287.

DOI: 10.1021/acs.inorgchem.5b01420
Inorg. Chem. 2015, 54, 8136−8147

(4) (a) He, X.; Yam, V. W.-W. *Coord. Chem. Rev.* **2011**, *255*, 2111. (b) Zhao, Q.; Li, F.; Huang, C. *Chem. Soc. Rev.* **2010**, *39*, 3007. (c) Guerchais, V.; Fillaut, J.-L. *Coord. Chem. Rev.* **2011**, *255*, 2448. (d) Ma, D.-L.; Ma, V. P.-Y.; Chan, D. S.-H.; Leung, K.-H.; He, H.-Z.; Leung, C.-H. *Coord. Chem. Rev.* **2012**, *256*, 3087.
(5) Sakamaki, D.; Ito, A.; Furukawa, K.; Kato, T.; Shiro, M.; Tanaka, K. *Angew. Chem., Int. Ed.* **2012**, *51*, 12776.
(6) Kurata, T.; Koshika, K.; Kato, F.; Kido, J.; Nishide, H. *Chem. Commun.* **2007**, 2986.
(7) (a) Yin, J.-F.; Velayudham, M.; Bhattacharya, D.; Lin, H.-C.; Lu, K.-L. *Coord. Chem. Rev.* **2012**, *256*, 3008. (b) Bomben, P. G.; Robson, K. C. D.; Koivisto, B. D.; Berlinguette, C. P. *Coord. Chem. Rev.* **2012**, *256*, 1438.
(8) (a) Creutz, C.; Taube, H. *J. Am. Chem. Soc.* **1969**, *91*, 3988. (b) Aguirre-Etcheverry, P.; O'Hare, D. *Chem. Rev.* **2010**, *110*, 4839. (c) Chisholm, M. H.; Lear, B. J. *Chem. Soc. Rev.* **2011**, *40*, 5254. (d) Low, P. J. *Coord. Chem. Rev.* **2013**, *257*, 1507. (e) Hankache, J.; Wenger, O. S. *Chem. Rev.* **2011**, *111*, 5138. (f) Heckmann, S.; Lambert, C. *Angew. Chem., Int. Ed.* **2012**, *51*, 326.
(9) (a) Keniley, L. K., Jr.; Dupont, N.; Ray, L.; Ding, J.; Kovnir, K.; Hoyt, J. M.; Hauser, A.; Shatruk, M. *Inorg. Chem.* **2013**, *52*, 8040. (b) Vajpayee, V.; Bivaud, S.; Goeb, S.; Croue, V.; Allain, M.; Popp, B. V.; Garci, A.; Therrien, B.; Salle, M. *Organometallics* **2014**, *33*, 1651. (c) Bellec, N.; Vacher, A.; Barriere, F.; Xu, Z.; Roisnel, T.; Lorcy, D. *Inorg. Chem.* **2015**, *54*, 5013. (d) Hu, L.; Liu, W.; Li, C.-H.; Zhou, X.-H.; Zuo, J.-L. *Eur. J. Inorg. Chem.* **2013**, *2013*, 6037. (e) Vacher, A.; Barriere, F.; Roisnel, T.; Lorcy, D. *Chem. Commun.* **2009**, 7200. (f) Vacher, A.; Barriere, F.; Roisnel, T.; Piekara-Sady, L.; Lorcy, D. *Organometallics* **2011**, *30*, 3570. (g) Vacher, A.; Barriere, F.; Lorcy, D. *Organometallics* **2013**, *32*, 6130.
(10) (a) Ji, Z.; Li, Y.; Pritchett, T. M.; Makarov, N. S.; Haley, J. E.; Li, Z.; Drobizhev, M.; Rebane, A.; Sun, W. *Chem. - Eur. J.* **2011**, *17*, 2479. (b) Li, H.-Y.; Wu, J.; Zhou, X.-H.; Kang, L.-C.; Li, D.-P.; Sui, Y.; Zhou, Y.-H.; Zheng, Y.-X.; Zuo, J.-L.; You, X.-Z. *Dalton Trans.* **2009**, 10563. (c) Adugna, S.; Revunova, K.; Djukic, B.; Gorelsky, S. I.; Jenkins, H. A.; Lemaire, M. T. *Inorg. Chem.* **2010**, *49*, 10183. (d) Hu, K.; Robson, K. C. D.; Johansson, P. G.; Berlinguette, C. P.; Meyer, G. J. *J. Am. Chem. Soc.* **2012**, *134*, 8352. (e) Nie, H.-J.; Chen, X.; Yao, C.-J.; Zhong, Y.-W.; Hutchison, G. R.; Yao, J. *Chem. - Eur. J.* **2012**, *18*, 14497. (f) Liu, J.; Zhang, Q.; Ding, H.-J.; Zhang, J.; Tan, J.-Y.; Wang, C.-K.; Wu, J.-Y.; Li, S.-L.; Zhou, H.-P.; Yang, J.-X.; Tian, Y.-P. *Sci. China: Chem.* **2013**, *56*, 1315. (g) Hu, K.; Robson, K. C. D.; Beauvilliers, E. E.; Schott, E.; Zarate, X.; Arratia-Perez, A.; Berlinguette, C. P.; Meyer, G. J. *J. Am. Chem. Soc.* **2014**, *136*, 1034.
(11) McClenaghan, N. D.; Passalacqua, R.; Loiseau, F.; Campagna, S.; Verheyde, B.; Hameurlaine, A.; Dehaen, W. *J. Am. Chem. Soc.* **2003**, *125*, 5356.
(12) (a) Sakuda, E.; Ando, Y.; Ito, A.; Kitamura, N. *Inorg. Chem.* **2011**, *50*, 1603. (b) Sun, Y.; Hudson, Z. M.; Rao, Y.; Wang, S. *Inorg. Chem.* **2011**, *50*, 3373. (c) Lee, Y. H.; Nghia, N. V.; Go, M. J.; Lee, J.; Lee, S. U.; Lee, M. H. *Organometallics* **2014**, *33*, 753.
(13) (a) Breivogel, A.; Kreitner, C.; Heinze, K. *Eur. J. Inorg. Chem.* **2014**, *2014*, 5468. (b) Wu, S.-H.; Shen, J.-J.; Yao, J.; Zhong, Y.-W. *Chem. - Asian J.* **2013**, *8*, 138. (c) Kowalski, K.; Linseis, M.; Winter, R. F.; Zabel, M.; Záliš, S.; Kelm, H.; Krüger, H.-J.; Sarkar, B.; Kaim, W. *Organometallics* **2009**, *28*, 4196. (d) Sato, M.; Shintate, H.; Kawata, Y.; Sekino, M.; Katada, M.; Kawata, S. *Organometallics* **1994**, *13*, 1956.
(14) (a) Mckinnon, S. D. J.; Patrick, B. O.; Lever, A. B. P.; Hicks, R. G. *J. Am. Chem. Soc.* **2011**, *133*, 13587. (b) Kusamoto, T.; Hattori, Y.; Tanushi, A.; Nishihara, H. *Inorg. Chem.* **2015**, *54*, 4186. (c) D'Avino, G.; Grisanti, L.; Guasch, J.; Ratera, I.; Veciana, J.; Painelli, A. *J. Am. Chem. Soc.* **2008**, *130*, 12064. (d) Ratera, I.; Veciana, J. *Chem. Soc. Rev.* **2012**, *41*, 303.
(15) (a) Kaim, W.; Sarkar, B. *Coord. Chem. Rev.* **2013**, *257*, 1650. (b) Moore, S. A.; Nagle, J. K.; Wolf, M. O.; Patrick, B. O. *Inorg. Chem.* **2011**, *50*, 5113. (c) Ceron-Camacho, R.; Hernandez, S.; Lagadec, R. L.; Ryabov, A. D. *Chem. Commun.* **2011**, *47*, 2823. (d) Chung, L.-H.; Chan, S.-C.; Lee, W.-C.; Wong, C.-Y. *Inorg. Chem.* **2012**, *51*, 8693. (e) Das, S.; Saha, D.; Mardanya, S.; Baitalik, S. *Dalton Trans.* **2012**, *41*, 12296. (f) Chang, S.-H.; Chang, C.-F.; Liao, J.-L.; Chi, Y.; Zhou, D.-Y.; Liao, L.-S.; Jiang, T.-Y.; Chou, T.-P.; Li, E. Y.; Lee, G. H.; Kuo, T.-Y.; Chou, P.-T. *Inorg. Chem.* **2013**, *52*, 5867. (g) Shao, J.-Y.; Zhong, Y.-W. *Inorg. Chem.* **2013**, *52*, 6464. (h) Sommer, M. G.; Schweinfurth, D.; Weisser, F.; Hohloch, S.; Sarkar, B. *Organometallics* **2013**, *32*, 2069. (i) Zheng, Q.-Y. *Sci. China: Chem.* **2014**, *57*, 1059. (i) Das, A.; Agarwala, H.; Kundu, T.; Ghosh, P.; Mondal, S.; Mobin, S. M.; Lahiri, G. K. *Dalton Trans.* **2014**, *43*, 13932. (j) Nie, H.-J.; Shao, J.-Y.; Yao, C.-J.; Zhong, Y.-W. *Chem. Commun.* **2014**, *50*, 10082. (k) Sun, M.-J.; Nie, H.-J.; Yao, J.-N.; Zhong, Y.-W. *Chin. Chem. Lett.* **2015**, *26*, 649. (l) Rajalakshmanan, E.; Alexander, V. *Inorg. Chem.* **2007**, *46*, 6252.
(16) Nie, H.-J.; Yao, C.-J.; Sun, M.-J.; Zhong, Y.-W.; Yao, J. *Organometallics* **2014**, *33*, 6223.
(17) (a) Yao, C.-J.; Yao, J.; Zhong, Y.-W. *Inorg. Chem.* **2011**, *50*, 6847. (b) Cui, B.-B.; Shao, J.-Y.; Zhong, Y.-W. *Organometallics* **2014**, *33*, 4220. (c) Yao, C.-J.; Zheng, R.-H.; Nie, H.-J.; Cui, B.-B.; Shi, Q.; Yao, J.; Zhong, Y.-W. *Chem. - Eur. J.* **2013**, *19*, 12376.
(18) Wang, J.; Hanan, G. S. *Synlett* **2005**, 1251.
(19) (a) Storrier, G. D.; Takada, K.; Abruna, H. D. *Inorg. Chem.* **1999**, *38*, 559. (b) Zhong, Y.-W.; Vila, N.; Henderson, J. C.; Flores-Torres, S.; Abruna, H. D. *Inorg. Chem.* **2007**, *46*, 10470.
(20) Sreenath, K.; Thomas, T. G.; Gopidas, K. R. *Org. Lett.* **2011**, *13*, 1134.
(21) (a) Beley, M.; Collin, J.-P.; Sauvage, J.-P.; Sugihara, H.; Heisel, F.; Miehe, A. *J. Chem. Soc., Dalton Trans.* **1991**, 3157. (b) Constable, E. C.; Thompson, A. M. W. C. *J. Chem. Soc., Dalton Trans.* **1994**, 1409.
(22) (a) Salaymeh, F.; Berhane, S.; Yusof, R.; de la Rosa, R.; Fung, E. Y.; Matamoros, R.; Lau, K. W.; Zheng, Q.; Kober, E. M.; Curtis, J. C. *Inorg. Chem.* **1993**, *32*, 3895. (b) Barlow, S. *Inorg. Chem.* **2001**, *40*, 7047. (c) Lambert, C.; Nöll, G. *J. Chem. Soc., Perkin Trans. 2* **2002**, 2039. (d) Santi, S.; Orian, L.; Durante, C.; Bisello, A.; Benetollo, F.; Crociani, L.; Ganis, P.; Ceccon, A. *Chem. - Eur. J.* **2007**, *13*, 1955. (e) Santi, S.; Durante, C.; Donoli, A.; Bisello, A.; Orian, L.; Ceccon, A.; Crociani, L.; Benetollo, F. *Organometallics* **2009**, *28*, 3319. (f) Shao, J.-Y.; Zhong, Y.-W. *Chem. - Eur. J.* **2014**, *20*, 8702.
(23) (a) Jones, S. C.; Coropceanu, V.; Barlow, S.; Kinnibrugh, T.; Timofeeva, T.; Brédas, J.-L.; Marder, S. R. *J. Am. Chem. Soc.* **2004**, *126*, 11782. (b) Ramirez, C. L.; Pegoraro, C. N.; Filevich, O.; Bruttomeso, A.; Etchenique, R.; Parise, A. R. *Inorg. Chem.* **2012**, *51*, 1261. (c) Sakamoto, R.; Sasaki, T.; Honda, N.; Yamamura, T. *Chem. Commun.* **2009**, 5156. (d) Parthey, M.; Vincent, K. B.; Renz, M.; Schauer, P. A.; Yufit, D. S.; Howard, J. A. K.; Kaupp, M.; Low, P. J. *Inorg. Chem.* **2014**, *53*, 1544.
(24) (a) Demadis, K. D.; Neyhart, G. A.; Kober, E. M.; White, P. S.; Meyer, T. J. *Inorg. Chem.* **1999**, *38*, 5948. (b) Demadis, K. D.; El-Samanody, E.-S.; Coia, G. M.; Meyer, T. J. *J. Am. Chem. Soc.* **1999**, *121*, 535.
(25) Zigler, D. F.; Mongelli, M. T.; Brewer, K. J. *Inorg. Chem. Commun.* **2007**, *10*, 295.
(26) Sheldrick, G. M. *Acta Crystallogr., Sect. A: Found. Crystallogr.* **2008**, *A64*, 112.
(27) Dolomanov, O. V.; Bourhis, L. J.; Gildea, R. J.; Howard, J. A. K.; Puschmann, H. *J. Appl. Crystallogr.* **2009**, *42*, 339.
(28) Lee, C.; Yang, W.; Parr, R. G. *Phys. Rev. B: Condens. Matter Mater. Phys.* **1988**, *37*, 785.
(29) Frisch, M. J.; Trucks, G. W.; Schlegel, H. B.; Scuseria, G. E.; Robb, M. A.; Cheeseman, J. R.; Montgomery, J. A., Jr.; Vreven, T.; Kudin, K. N.; Burant, J. C.; Millam, J. M.; Iyengar, S. S.; Tomasi, J.; Barone, V.; Mennucci, B.; Cossi, M.; Scalmani, G.; Rega, N.; Petersson, G. A.; Nakatsuji, H.; Hada, M.; Ehara, M.; Toyota, K.; Fukuda, R.; Hasegawa, J.; Ishida, M.; Nakajima, T.; Honda, Y.; Kitao, O.; Nakai, H.; Klene, M.; Li, X.; Knox, J. E.; Hratchian, H. P.; Cross, J. B.; Adamo, C.; Jaramillo, J.; Gomperts, R.; Stratmann, R. E.; Yazyev, O.; Austin, A. J.; Cammi, R.; Pomelli, C.; Ochterski, J. W.; Ayala, P. Y.; Morokuma, K.; Voth, G. A.; Salvador, P.; Dannenberg, J. J.; Zakrzewski, V. G.; Dapprich, S.; Daniels, A. D.; Strain, M. C.; Farkas, O.; Malick, D. K.; Rabuck, A. D.; Raghavachari, K.; Foresman, J. B.; Ortiz, J. V.; Cui, Q.; Baboul, A. G.; Clifford, S.; Cioslowski, J.; Stefanov, B. B.; Liu, G.; Liashenko, A.; Piskorz, P.; Komaromi, I.;

DOI: 10.1021/acs.inorgchem.5b01420
Inorg. Chem. 2015, 54, 8136−8147

Martin, R. L.; Fox, D. J.; Keith, T.; Al-Laham, M. A.; Peng, C. Y.; Nanayakkara, A.; Challacombe, M.; Gill, P. M. W.; Johnson, B.; Chen, W.; Wong, M. W.; Gonzalez, C.; Pople, J. A. *Gaussian 09*, revision A.2; Gaussian, Inc.: Wallingford, CT, 2009.
(30) (a) Dunning, T. H.; Hay, P. J. In *Modern Theoretical Chemistry*; Schaefer, H. F., Ed.; Plenum: New York, 1976; Vol. 3, p 1. (b) Hay, P. J.; Wadt, W. R. *J. Chem. Phys.* **1985**, *82*, 299.
(31) (a) Andzelm, J.; Kölmel, C.; Klamt, A. *J. Chem. Phys.* **1995**, *103*, 9312. (b) Barone, V.; Cossi, M. *J. Phys. Chem. A* **1998**, *102*, 1995.

DOI: 10.1021/acs.inorgchem.5b01420
Inorg. Chem. 2015, 54, 8136−8147